**Rare Metal Materials and Engineering**
Volume 52, Issue 3, March 2023
Available online at www.rmme.ac.cn

Science Press

**Cite this article as**: Jing Zhenquan, Sun Yanhui, Liu Rui, et al. Effect of Vacuum Arc Remelting Process Parameters on Macrosegregation in TC4 Titanium Alloy[J]. Rare Metal Materials and Engineering, 2023, 52(03): 815-822.

ARTICLE

# Effect of Vacuum Arc Remelting Process Parameters on Macrosegregation in TC4 Titanium Alloy

**Jing Zhenquan[1], Sun Yanhui[1], Liu Rui[1], Chen Lian[2], Geng Naitao[3], Zheng Youping[3], Peng Li[3], Wang Ying[3]**

*[1] Collaborative Innovation Center of Steel Technology, University of Science and Technology Beijing, Beijing 100083, China; [2] Pangang Group Panzhihua Research Institute of Iron and Steel Co., Ltd, Panzhihua 617000, China; [3] Chengdu Advanced Metal Materials Industrial Technology Research Institute Co., Ltd, Chengdu 610300, China*

**Abstract:** Fluent software was used to simulate the interaction among the temperature field, flow field, and solute field in the vacuum arc remelting process of TC4 titanium alloy. The effects of three process parameters (smelting rate, upper surface temperature of the ingot, and cooling intensity), which are directly related to the ingot, on the ingot macrosegregation were studied. Results show that under different smelting conditions, the radial macrosegregation of Fe element shows a bell-shaped distribution at the ingot height of 1000 mm, i. e., the core of ingot presents the positive macrosegregation whereas the surface area presents the negative macrosegregation, and the degree of negative macrosegregation is greater than that of the positive macrosegregation. The effect of smelting rates on the temperature field and macrosegregation of the ingot is the most obvious: with increasing the smelting rate from 0.15 mm/s to 0.18 mm/s, the ingot height to reach the stable melting stage is increased from 1200 mm to 1600 mm, and the depth of the molten pool is increased from 494 mm to 738 mm. In the area within the distance of 130 mm from the ingot center, the macrosegregation is decreased with increasing the smelting rate, and the maximum value is 3.36% when the smelting rate is 0.15 mm/s. In the area beyond the distance of 295 mm from the ingot center, the macrosegregation is increased with increasing the smelting rate, and the maximum value is 6.23% when the smelting rate is 0.21 mm/s. The effect of upper surface temperature and cooling intensity on macrosegregation and molten pool depth is not obvious. Through the orthogonal analysis, the influence degree of three main process parameters on macrosegregation is as follows: smelting rate>cooling intensity>ingot upper surface temperature. The optimal conditions are smelting rate of 0.15 mm/s, ingot upper surface temperature of 2179 K, and cooling intensity of 500 (bottom)/1000 (side) $W \cdot m^{-2} \cdot K^{-1}$.

**Key words:** titanium alloy; vacuum arc remelting; numerical simulation; macrosegregation

Because of their remarkable advantages, such as high specific strength, good corrosion resistance, and high melting point, titanium alloys are widely used in aerospace, equipment manufacturing, medical equipment, and sporting goods[1]. Among them, the typical $\alpha+\beta$ two-phase titanium alloy (TC4) has good process plasticity and excellent comprehensive performance, which is suitable for various pressure forming. Therefore, TC4 alloy has various complete varieties and specifications in industrial production[1–3].

Currently, vacuum arc remelting (VAR) is the main production method for titanium alloy ingots, because of its simple equipment requirement, low cost, and easy operation. The basic feature of VAR is that the consumable electrode continuously melts while the ingot continuously solidifies and increases in the mold[3–4]. During the smelting process, the cooling conditions and the shape/depth of the molten pool are not stable, and the distribution coefficients of alloying elements during solidification are different, which inevitably enriches the alloying elements and forms macrosegregation. According to the crystal macrosegregation theory, the equilibrium partition coefficient $k$ of the solute element determines the macrosegregation degree. When $k$<1, the positive macrosegregation occurs; when $k$>1, the negative macrosegregation occurs. The further the $k$ value deviates

Received date: September 11, 2022
Corresponding author: Sun Yanhui, Ph. D., Professor, Collaborative Innovation Center of Steel Technology, University of Science and Technology Beijing, Beijing 100083, P. R. China, E-mail: ustbsyh801@163.com

from 1, the greater the macrosegregation degree. The coefficient $k$ of Fe element in titanium alloy is 0.3, presenting a great tendency of macrosegregation[5–8]. During VAR, the melting process parameters are the key factors to control the ingot quality. A reasonable smelting process can reduce the defects caused by the smelting process and improve the qualified rate of product. In VAR process, the relevant process parameters are smelting rate, smelting current, smelting voltage, furnace vacuum, cooling water flow, and temperature[9].

Due to the high cost of industrial testing of titanium alloy production and the difficulty in observation of ingot variation during VAR process, the numerical calculation gradually replaces the traditional trial-and-error method to study the solidification structure. Numerical calculation not only directly simulates the formation of solidified structure, but also clarifies the formation mechanism of solidified structure[10–14].

In this research, Fluent software, as the fluid dynamics calculation software based on the finite volume method, was used to simulate the interactions among temperature field, flow field, and solute field in VAR process. Meanwhile, due to the restrictions of numerical simulation, the influence of three process parameters which are directly related to ingots (smelting rate, ingot upper surface temperature, and cooling intensity) was investigated.

## 1 Experiment

The raw materials of ingots in this study were composed of small-sized sponge titanium (0A grade), AlV55 alloy, aluminum particles, $TiO_2$ powder, and titanium-iron alloy. An automatic weighing system was used to weigh the titanium sponge, Al particles, and AlV55 alloy, and an electronic scale was used to weigh the $TiO_2$ powder and titanium-iron alloy. These raw materials were mixed by a mixer and then poured into the press with load of 80 MN to produce the electrode block with diameter of 470 mm and height of 190 mm. Electrode welding was conducted in a vacuum plasma welding box. In order to avoid the material waste, the melting was conducted three times after the sampling of the secondary ingot. The diameters of the primary, secondary, and tertiary smelting crucibles were 570, 660, and 750 mm, respectively. The ingot should be turned around before the next smelting. The main production process was as follows: sponge titanium raw materials→pressed electrode block→electrode stacking→vacuum plasma welding→first smelting→ingot cleaning→second smelting→ingot cleaning→third smelting.

The secondary ingot was cut along the red lines in Fig. 1a. The ingot specimen was cut at the middle part, and a disk specimen with thickness of 20–25 mm was obtained at the middle section. After the specimen was corroded, the specimen composition was analyzed through the measurement points, as shown in Fig.1b.

## 2 Numerical Simulation

### 2.1 Mathematical model

Due to the symmetry of cylindrical ingot, it is simplified to a two-dimensional rectangle. Because the thermal conductivity of the copper crucible is much higher than that of the titanium alloy ingot, the influence of copper crucible can be neglected for the heat dissipation of ingot during the simulation. The main models used in numerical simulation calculation were energy model, flow model, component transport model, and the solidification-melting model. The continuous growth of ingot is realized through the dynamic grid method[15–16].

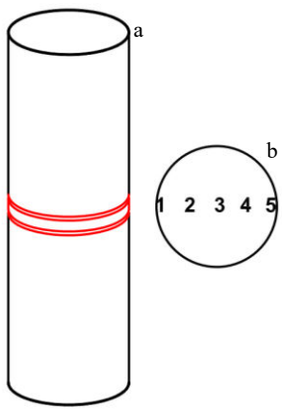


Fig.1 Schematic diagrams of secondary ingot sampling: (a) disk specimen from secondary ingot and (b) composition analysis points

(1) Governing equation

The main equations used in the model are continuity equation, momentum equation, energy equation, and solute transport equation, as expressed by Eq.(1–4), respectively:

$$\frac{\partial \rho}{\partial t} + \nabla \cdot (\rho u) = 0 \tag{1}$$

$$\rho \frac{\partial u_i u_j}{\partial x_j} = \frac{\partial}{\partial x_j}\left[\mu_{\text{eff}}\left(\frac{\partial u_i}{\partial x_j} + \frac{\partial u_j}{\partial x_i}\right)\right] - \frac{\partial P}{\partial x_i} + \rho g_i + F_{\text{B}} + S_{\text{P}} \tag{2}$$

$$\rho u_i \frac{\partial H}{\partial x_i} = \frac{\partial}{\partial x_i}\left[\left(k_{\text{l}} + \frac{\mu_{\text{t}}}{Pr_{\text{t}}}\right)\frac{\partial T}{\partial x_i}\right] \tag{3}$$

$$\rho \frac{\partial Y_m}{\partial t} + \rho \frac{\partial u_i Y_m}{\partial x_i} = \frac{\partial}{\partial x_i}\left[\rho\left(D_{\text{L},m} + \frac{\mu_{\text{t}}}{Sc_{\text{t}}}\right)\frac{\partial Y_m}{\partial x_i}\right] + S_{i,\text{dif}} + S_{i,\text{con}} \tag{4}$$

where $t$ is time; $x$ is spatial coordinate; $u$ is velocity component along $x$ direction ($\text{m}\cdot\text{s}^{-1}$); the subscripts $i$ and $j$ represent different directions; $\rho$ is density ($\text{kg}\cdot\text{m}^{-3}$); $P$ is pressure (Pa); $g_i$ is gravitational acceleration ($\text{m}\cdot\text{s}^{-2}$); $F_{\text{B}}$ denotes the thermal buoyancy; $S_{\text{P}}$ accounts for the phase interaction force within the mushy zone; $\mu_{\text{eff}}$ is effective viscosity coefficient; $k_{\text{l}}$ is thermal conductivity of melt laminar flow ($\text{W}\cdot\text{m}^{-1}\cdot\text{K}^{-1}$); $Pr_{\text{t}}$ is turbulent Prandtl number (0.85); $\mu_{\text{t}}$ denotes turbulent viscosity; $T$ denotes temperature (K); $H$ is total enthalpy of the system; $Y_m$ is the $m$ solute content (wt%); $D_{\text{L},m}$ is diffusion coefficient of the component $m$ in liquid phase ($\text{m}^2\cdot\text{s}^{-1}$); $Sc_{\text{t}}$ is turbulent Schmidt number (1.0); $S_{i,\text{dif}}$ and $S_{i,\text{con}}$ are the diffusion source term and the convection source term, respectively.

(2) Boundary conditions

The main boundary conditions in the calculation process

are as follows. The upper surface of the ingot is the velocity inlet, other boundaries are non-slip boundaries, and there is no solute exchange between the walls and the outside. The bottom and side walls of the ingot are convective heat transfer boundaries. The temperature of the ingot upper surface ($T$) is as follows:

$$T = T_L + 400e^{-\frac{12D_c}{J}} \quad (5)$$

where $T_L$ is liquidus temperature (K); $J$ is melting current (kA); $D_c$ is the ingot diameter (m).

The schematic diagrams of ingot model and meshing in this study are shown in Fig.2. The ingot diameter is 660 mm, the initial height of ingot is 50 mm, and the final height is 2000 mm. A square grid with a side length of 2 mm is used.

(3) Simulation parameters

The relevant physical parameters used in this model are shown in Table 1[17].

### 2.2 Model validation

To ensure the accuracy of the mathematical model, the calculation results of the numerical simulation were compared with the experiment results, as shown in Fig.3. It can be seen that the numerical simulation results are in good agreement with the experiment results, indicating that the numerical simulation model is reliable.

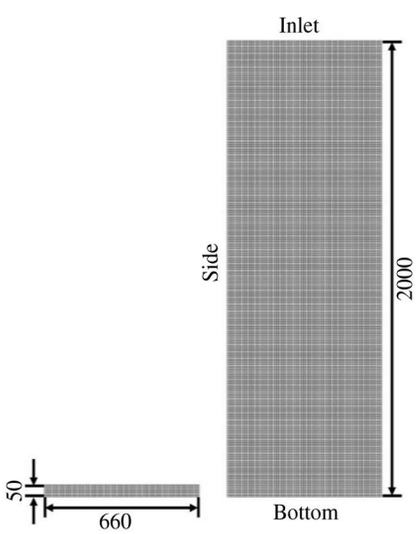


Fig.2 Schematic diagrams of ingot model and meshing at initial state (a) and final state (b)

**Table 1 Relevant physical parameters of TC4 alloy for simulation model[17]**

| Parameter | Value |
|---|---|
| Density/kg·m$^{-3}$ | 3925 |
| Thermal conductivity/W·(m·K)$^{-1}$ | 29.7 |
| Pure solvent melting heat/J·kg$^{-1}$ | 330 000 |
| Specific heat/J·(kg·K)$^{-1}$ | 727 |
| Viscosity/kg·m·s$^{-1}$ | 0.0026 |
| Slope of liquidus line/K·wt%$^{-1}$ | 18 |
| Thermal expansion coefficient/K$^{-1}$ | 6.5×10$^{-5}$ |
| Solute expansion coefficient | −0.75 |
| Mass diffusivity/m$^2$·s$^{-1}$ | 3×10$^{-9}$ |
| Partition coefficient | 0.3 |

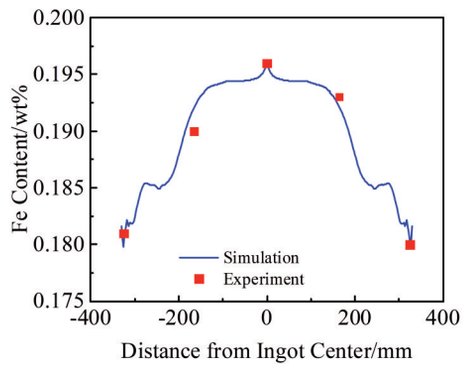


Fig.3 Comparison between numerical simulation results and experiment results

### 2.3 Calculation scheme

In this research, the effects of melting process parameters on macrosegregation of ingots were studied from three aspects: smelting rate, upper surface temperature, and cooling intensity. In order to quantitatively analyze the role of these three parameters, seven calculation schemes were used for comparison in the simulation calculation, as shown in Table 2.

## 3 Results and Discussion

### 3.1 Variations of temperature field and solute field at different heights of ingots during smelting

According to Scheme 2, the changes of temperature field and solute field of ingots with different heights during smelting are obtained, as shown in Fig. 4 and Fig. 5, respectively.

As shown in Fig. 4a, since the crucible bottom can effectively cool the molten pool at the beginning of smelting, the molten metal rapidly solidifies and forms a flat shallow molten pool. With the ingot gradually forming, the heat dissipated through the crucible is less than the heat released by the solidification of molten metal. Therefore, the heat accumulation results in the deepening of molten pool, as shown in Fig.4b and 4c. Since the middle area of the molten

**Table 2 Calculation schemes for different smelting processes**

| Calculation scheme | Smelting rate/mm·s$^{-1}$ | Upper surface temperature/K | Cooling intensity/ W·m$^{-2}$·K$^{-1}$ | |
|---|---|---|---|---|
| | | | Bottom | Side |
| 1 | 0.15 | 2179.1 | 600 | 1100 |
| 2 | 0.18 | 2179.1 | 600 | 1100 |
| 3 | 0.21 | 2179.1 | 600 | 1100 |
| 4 | 0.18 | 2151.0 | 600 | 1100 |
| 5 | 0.18 | 2198.3 | 600 | 1100 |
| 6 | 0.18 | 2179.1 | 500 | 1000 |
| 7 | 0.18 | 2179.1 | 700 | 1200 |

pool is far away from the crucible, the heat accumulation phenomenon is the most obvious. The shape of the molten pool gradually evolves from flat shape to funnel shape. When the generation and dissipation of heat in the crucible gradually reaches a balance state, a stable molten pool forms, and the stable smelting stage is achieved, as shown in Fig. 4b and 4c. After that, the shape and depth of the melt pool hardly changes, as shown in Fig.4e.

At the beginning of smelting process, the molten pool is rapidly cooled through the bottom and side walls. The cooling rate is fast, and thus the solute has no time to segregate, resulting in the formation of ingot with a more uniform structure, as shown in Fig.5a. With increasing the ingot height, the solute content in the core is gradually increased, forming a positive macrosegregation. Therefore, a fishtail macrosegregation occurs in the lower part of the ingot, as shown in Fig. 5a and 5b. With the formation of stable molten pool, the composition distribution from the edge to the core is gradually stabilized, and the solute component at the solidification front is gradually accumulated, forming a necklace-like center macrosegregation, as shown in Fig.5c and 5d. At the capping stage of ingot formation, the molten pool is cooled by the top and side walls at the same time. Thus, the solute has no time to diffuse, forming an inverted fishtail macrosegregation with a higher concentration of solute, as shown in Fig.5e.

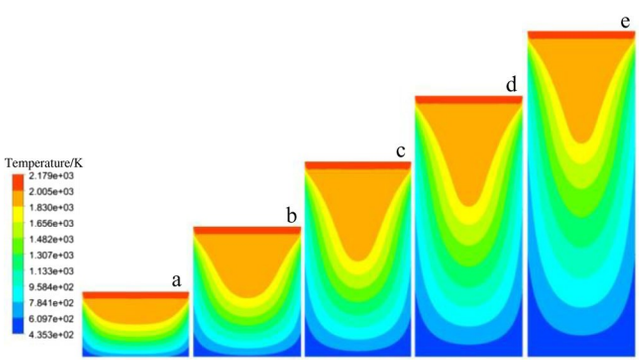


Fig.4 Variation of temperature field of ingots with different heights during smelting: (a) 400 mm, (b) 800 mm, (c) 1200 mm, (d) 1600 mm, and (e) 2000 mm

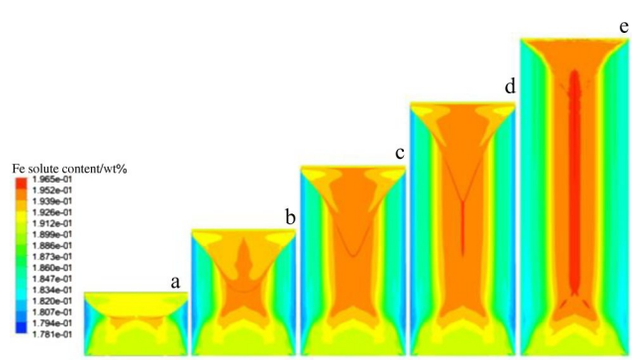


Fig.5 Variation of solute field of ingots with different heights during smelting: (a) 400 mm, (b) 800 mm, (c) 1200 mm, (d) 1600 mm, and (e) 2000 mm

Fig. 6 shows the variation of Fe macrosegregation in ingots at different heights after smelting. It can be seen that the Fe macrosegregation in ingots at different heights all presents a bell shape. With increasing the height from 200 mm to 1000 mm, the core macrosegregation is gradually increased. The core composition of the bottom (200 mm) and top (1800 mm) sides of the ingots is relatively uniform, whereas that of the middle part (heights at 600, 1000, and 1400 mm) of the ingots fluctuates greatly. In addition, the most depleted part of the solute is not at the outer surface of the ingot, but at the area with a certain distance from the outer surface. Because the outer surface of the ingot solidifies rapidly under the chilling of the crucible wall, there is no time for the solute transport. Thus, the macrosegregation composition is relatively uniform. The cooling rate is decreased with increasing the distance from the outer surface, and thereby the melt flow in the molten pool is increased, resulting in the depleted solutes.

### 3.2 Effects of smelting rate, upper surface temperature, and cooling intensity on temperature field and solute field

#### 3.2.1 Effect of smelting rate on temperature field and macrosegregation

The smelting rate can significantly influence the physical properties of product during the smelting process. Therefore, it is of great significance to analyze the influence of the smelting rate on macrosegregation. In Scheme 1, 2, and 3, the upper surface temperature and cooling intensity are fixed, and the smelting rate is 0.15, 0.18, and 0.21 mm/s, respectively. Fig. 7 shows the temperature field distributions in the ingots with height of 2000 mm at different smelting rates. It can be seen that with increasing the smelting rate, the isotherm at the ingot center moves significantly downward, and the depth of the liquid phase cavity is increased.

Fig. 8 shows the change of liquid core depths at the ingot center under different smelting rates. It can be seen that with increasing the ingot height, the depth of the liquid core at the ingot center is firstly increased and then remains unchanged,

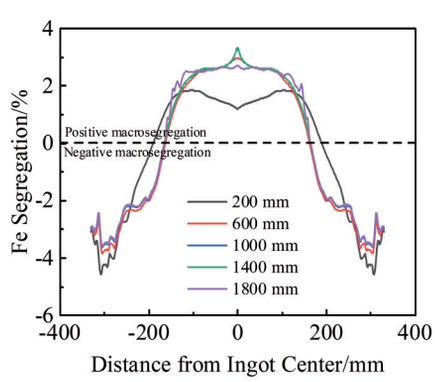


Fig.6 Variation of Fe macrosegregation in ingots at different heights after smelting

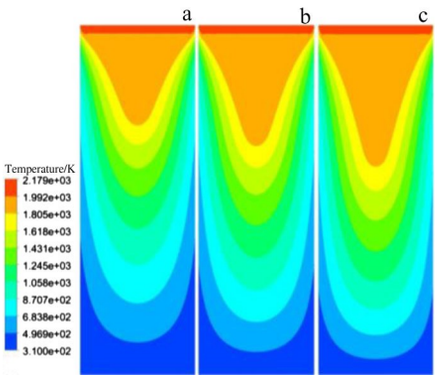


Fig.7 Temperature field distributions in ingots with height of 2000 mm at different smelting rates: (a) 0.15 mm/s, (b) 0.18 mm/s, and (c) 0.21 mm/s

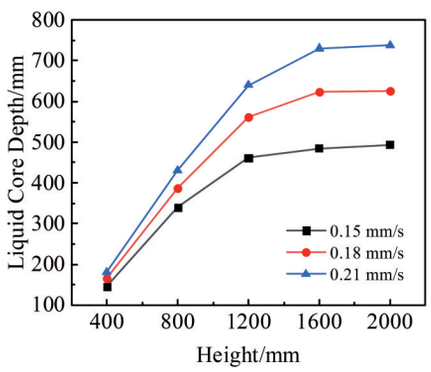


Fig.8 Variation of liquid core depths at ingot center under different smelting rates

indicating that the ingot finally reaches a stable smelting stage. When the smelting rate is 0.15, 0.18, and 0.21 mm/s, the ingot reaches the stable melting stage at height of 1200, 1600, and over 1600 mm, respectively. This result suggests that with increasing the smelting rate, the height for stable smelting stage is gradually increased. At the stable smelting stage, the depth of the liquid core at the ingot center under the smelting rate of 0.15, 0.18, and 0.21 mm/s is 494, 626, and 738 mm, respectively. Therefore, the increment in liquid core depth becomes smaller with increasing the smelting rate. Briefly, with increasing the smelting rate, the height for stable smelting stage is increased, and the depth of the liquid core is increased significantly with a decreased increment.

In order to compare the influence of different smelting rates on the macrosegregation in ingots, the macrosegregation of Fe element in ingot at height of 1000 mm was compared, as shown in Fig.9. It can be seen that the Fe macrosegregation in ingots under different smelting rates all shows a bell-shape distribution. Positive macrosegregation occurs in the area within the distance of 175 mm from the ingot center, and when the smelting rate is 0.15 mm/s, the maximum value of positive macrosegregation is 3.36%. The negative macrosegregation occurs in the area beyond the distance of 195 mm from the ingot center, and the maximum value of negative

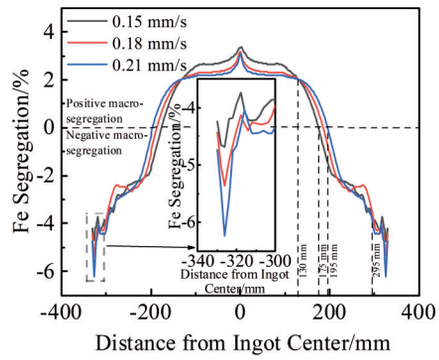


Fig.9 Variation of Fe macrosegregation in ingots at height of 1000 mm under different smelting rates

macrosegregation is 6.23% when the smelting rate is 0.21 mm/s. Although the smelting rates are different, the degree of negative macrosegregation is all greater than that of positive macrosegregation. In the outer surface area of ingot (distance >295 mm from the ingot center), the macrosegregation is increased with increasing the smelting rate. When the smelting rate increases from 0.15 mm/s to 0.18 mm/s, the macrosegregation is increased from 4.69% to 6.23%. In the central region of the ingot (distance<130 mm from the ingot center), the macrosegregation is decreased with increasing the smelting rate. When the smelting rate increases from 0.15 mm/s to 0.18 mm/s, the macrosegregation is decreased from 3.36% to 3.05%.

### 3.2.2 Influence of upper surface temperature on temperature field and macrosegregation

According to Eq. (5), the relationship between the current and the upper surface temperature of the ingot, when the ingot diameter is 660 mm and the melting current is 17, 22, and 27 kA, the upper surface temperature of the ingot is 2151, 2179, and 2198 K, respectively.

In Scheme 4, 2, and 5, the smelting rate and cooling intensity are fixed, and the upper surface temperature of the ingot is 2151, 2179, and 2198 K, respectively. As shown in Fig. 10, with increasing the upper surface temperature of the ingot, there is no obvious change in the temperature field of the molten pool.

Fig.11 shows the variation of liquid core depths in ingots at different heights under different upper surface temperatures. It

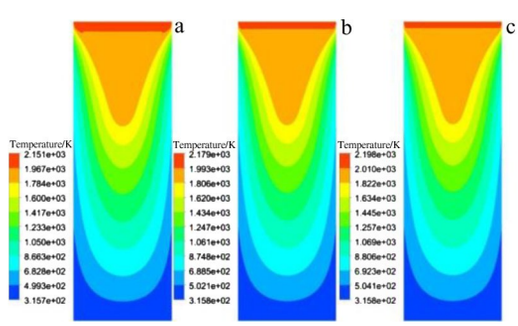


Fig.10 Temperature field distributions at different upper surface temperatures: (a) 2151 K, (b) 2179 K, and (c) 2198 K

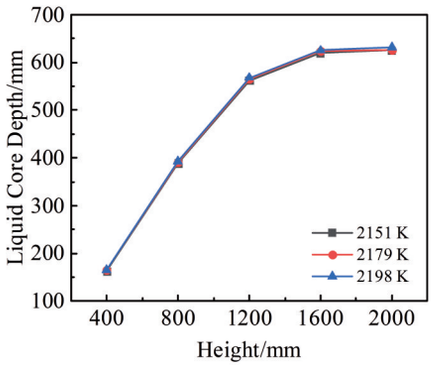


Fig.11 Variation of liquid core depth in ingots at different upper surface temperatures

can be seen that with increasing the height of ingot, the liquid core depth at the ingot center is firstly increased and then reaches a stable stage. When the ingot reaches the stable melting stage with the ingot upper surface temperature of 2151, 2179, and 2198 K, the liquid core depth at the ingot center is 626, 626, and 632 mm, respectively, but their difference is slight. The average depth is 626 mm.

Fig.12 shows the variation of Fe macrosegregation in ingots at height of 1000 mm under different upper surface temperatures. It can be seen that the macrosegregation distributions are basically the same under different upper surface temperatures. In the area within the distance of 185 mm from the ingot center, the positive macrosegregation occurs, and the maximum value of positive macrosegregation is 3.20%. Beyond that area, the negative macrosegregation can be observed, and the maximum value of negative macrosegregation is 5.70%. In the area beyond the distance of 300 mm from the ingot center, with increasing the upper surface temperature of the ingot from 2151 K to 2198 K, the maximum value of negative macrosegregation is decreased from 5.70% to 5.30%.

3.2.3 Effect of cooling intensity on temperature field and macrosegregation

Under the same conditions of smelting rate and upper surface temperature of ingot, the effects of cooling intensities on the macrosegregation of ingot were analyzed through

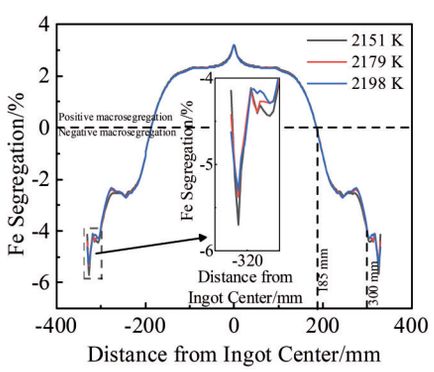


Fig.12 Variation of Fe macrosegregation in ingots at height of 1000 mm under different upper surface temperatures

Scheme 2, 6, and 7. It can be seen from Fig. 13 that the temperature field of the ingot does not change significantly under different cooling intensities.

Fig. 14 also infers that the effect of cooling intensity on the liquid core depth at the ingot center is not obvious. After the ingot reaches the stable melting stage, with increasing the cooling intensity from 500 (bottom)/1000 (side) $W \cdot m^{-2} \cdot K^{-1}$ to 700 (bottom)/1200 (side) $W \cdot m^{-2} \cdot K^{-1}$, the liquid core depth at the ingot center is slightly increased from 626 mm to 630 mm. The average depth is 628 mm.

According to Fig. 15, the macrosegregation is basically the same under different cooling intensities. The positive macrosegregation occurs in the area within the distance of 185 mm from the ingot center, and the maximum value of positive macrosegregation is 3.18%. Beyond that area, the negative macrosegregation occurs, and its maximum value is 5.72%. Thus, the degree of negative macrosegregation is greater than that of the positive macrosegregation. With increasing the cooling intensity from 500/1000 $W \cdot m^{-2} \cdot K^{-1}$ to 700/1200 $W \cdot m^{-2} \cdot K^{-1}$, the maximum value of negative macrosegregation is increased from 4.88% to 5.72% in the area beyond the distance of 305 mm from ingot center.

### 3.3 Determination of optimal parameters

According to the abovementioned results, it can be

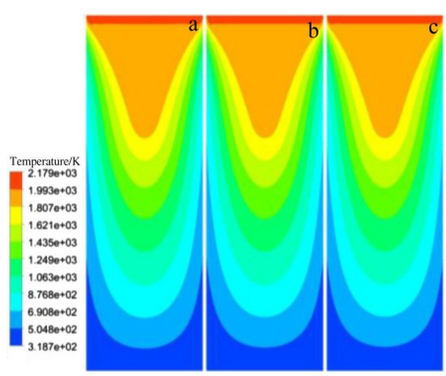


Fig.13 Temperature field distributions under different cooling intensities: (a) 500/1000 $W \cdot m^{-2} \cdot K^{-1}$, (b) 600/1100 $W \cdot m^{-2} \cdot K^{-1}$, and (c) 700/1200 $W \cdot m^{-2} \cdot K^{-1}$

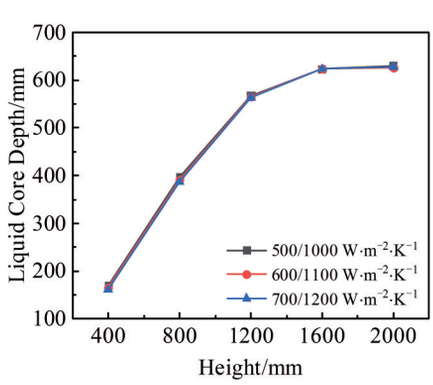


Fig.14 Variation of liquid core depth under different cooling intensities

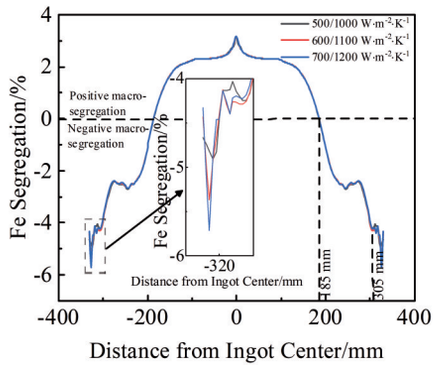


Fig.15 Variation of Fe macrosegregation in ingots at height of 1000 mm under different cooling intensities

**Table 3 Orthogonal experiment conditions**

| Level | Smelting rate/mm·s$^{-1}$ | Upper surface temperature/K | Cooling intensity/ W·m$^{-2}$·K$^{-1}$ | |
|---|---|---|---|---|
| | | | Bottom | Side |
| 1 | 0.15 | 2151 | 500 | 1000 |
| 2 | 0.18 | 2179 | 600 | 1100 |
| 3 | 0.21 | 2198 | 700 | 1200 |

**Table 4 Orthogonal experiment results and numerical simulation results of the influence of smelting rate, upper surface temperature of ingot, and cooling intensity on macrosegregation**

| Case | Smelting rate/ mm·s$^{-1}$ | Upper surface temperature/ K | Cooling intensity/ W·m$^{-2}$·K$^{-1}$ | | Maximum macrosegregation/% |
|---|---|---|---|---|---|
| | | | Bottom | Side | |
| 1 | 0.15 | 2151 | 500 | 1000 | −4.72 |
| 2 | 0.15 | 2179 | 600 | 1100 | −4.75 |
| 3 | 0.15 | 2198 | 700 | 1200 | −5.00 |
| 4 | 0.18 | 2151 | 600 | 1100 | −5.70 |
| 5 | 0.18 | 2179 | 700 | 1200 | −5.72 |
| 6 | 0.18 | 2198 | 500 | 1000 | −5.37 |
| 7 | 0.21 | 2151 | 700 | 1200 | −6.12 |
| 8 | 0.21 | 2179 | 500 | 1000 | −5.39 |
| 9 | 0.21 | 2198 | 600 | 1100 | −5.62 |
| $K_1$ | −14.47 | −16.54 | −15.48 | | - |
| $K_2$ | −16.79 | −15.86 | −16.07 | | - |
| $K_3$ | −17.13 | −15.99 | −16.84 | | - |
| $k_1$ | −4.82 | −5.51 | −5.16 | | - |
| $k_2$ | −5.60 | −5.29 | −5.36 | | - |
| $k_3$ | −5.71 | −5.33 | −5.61 | | - |
| $R$ | 0.887 | 0.227 | 0.453 | | - |

Note: $K_1$, $K_2$ and $K_3$ represent the sum of segregation degrees of each factor at Level 1, Level 2, and Level 3, respectively; $k_1$, $k_2$, and $k_3$ represent the average macrosegregation degree of each factor at Level 1, Level 2, and Level 3, respectively; $R$ represents the range of the average level of each influence factor.

concluded that the negative macrosegregation in the outer surface is more serious than the positive macrosegregation in the central surface of the ingots.

In order to compare the influence degree of smelting rate, upper surface temperature of ingot, and cooling intensity on the macrosegregation, the orthogonal experiments were conducted with the maximum macrosegregation as the evaluation index of the melting effect, as listed in Table 3. In addition, the optimal operating conditions under the existing process can also be obtained.

The orthogonal experiment was designed by the L9(34) type table, as shown in Table 4, and the numerical simulation results are also shown in Table 4 for comparison.

According to Table 4, the optimal process parameters can be obtained. The range value $R$ can reflect the influence on the experiment results when the factor range fluctuates. According to the magnitude of the range, it can be deduced that the influence degree on macrosegregation is as follows: smelting rate>cooling intensity>upper surface temperature of the ingot, which is consistent with the calculation results. Besides, according to the $k_1$, $k_2$, and $k_3$ values, it can be concluded that the optimal process parameters under the current working conditions are smelting rate of 0.15 mm/s, ingot upper surface temperature of 2179 K, and cooling intensity of 500 (bottom)/ 1000 (side) W·m$^{-2}$·K$^{-1}$.

## 4 Conclusions

1) The influence of smelting rate on the temperature field and macrosegregation of the TC4 alloy ingot is the most obvious. With increasing the smelting rate from 0.15 mm/s to 0.18 mm/s, the ingot height to reach the stable melting stage is increased from 1200 mm to 1600 mm, and the molten pool depth is increased from 494 mm to 738 mm. Under different smelting rates, the Fe macrosegregation in ingot at height of 1000 mm shows a bell-shape distribution. In the area within the distance of 130 mm from the ingot center, the macrosegregation is decreased with increasing the smelting rate, and the maximum macrosegregation value is 3.36% at smelting rate of 0.15 mm/s. In the area beyond the distance of 295 mm from ingot center, the macrosegregation is increased with increasing the smelting rate, and the maximum macrosegregation value is 6.23% at smelting rate of 0.21 mm/s.

2) The upper surface temperature of ingot has slight effect on the temperature field and macrosegregation. When the upper surface temperature of ingot increases from 2151 K to 2198 K, the molten pool depth barely changes at the stable melting stage, and the average depth is about 626 mm. In the area within the distance of 185 mm from the ingot center, positive macrosegregation occurs, and its maximum value is 3.20%. In the area beyond the distance of 185 mm from ingot center, the maximum value of negative macrosegregation is decreased from 5.70% to 5.30% with increasing the upper surface temperature of ingot from 2151 K to 2198 K.

3) The influence of cooling intensity on temperature field and macrosegregation is not obvious. With increasing the

cooling intensity, the liquid core depth of the ingot at the stable melting stage changes slightly, and the average depth is 628 mm. In the area within the distance of 185 mm from the ingot center, the positive macrosegregation occurs, and the maximum value of positive macrosegregation is 3.18%. The maximum value of negative macrosegregation is increased from 4.88% to 5.72% with increasing the cooling intensity from 500 (bottom)/1000 (side) $W\cdot m^{-2}\cdot K^{-1}$ to 700 (bottom)/1200 (side) $W\cdot m^{-2}\cdot K^{-1}$.

4) The influence degree of the process parameters on the macrosegregation is smelting rate>cooling intensity>upper surface temperature of the ingot. The optimal conditions are smelting rate of 0.15 mm/s, ingot upper surface temperature of 2179 K, and cooling intensity of 500 (bottom)/1000 (side) $W\cdot m^{-2}\cdot K^{-1}$.

## References


1 Guo Li, He Weixia, Zhou Peng *et al*. *Hot Working Technology* [J], 2020, 49(22): 22 (in Chinese)

2 Dong Jian, Chen Ji, Wang Dan *et al*. *Metallurgy and Materials*[J], 2014, 34(2): 6 (in Chinese)

3 Yuan Wei. *Nonferrous Metals Processing*[J], 2018, 47(2): 23 (in Chinese)

4 Lei Wenguang, Zhao Yongqing, Han Dong *et al*. *Materials Reports*[J], 2016, 30(3): 101 (in Chinese)

5 Gao Ping, Zhao Yongqing, Mao Xiaonan *et al*. *Titanium Industry Progress*[J], 2009, 26(1): 1 (in Chinese)

6 Lai Meixiang, Tang Hongguo, Yi Binghua *et al*. *Ferro-Alloys*[J], 2008(3): 9 (in Chinese)

7 Zhao Yongqing, Liu Junlin, Zhou Lian. *Rare Metal Materials and Engineering*[J], 2005, 34(4): 531 (in Chinese)

8 Du Yujun, Liu Xianghong, Li Jinshan *et al*. *Rare Metal Materials and Engineering*[J], 2020, 49(3): 883 (in Chinese)

9 Zou Wuzhuang. *Titanium Industry Progress*[J], 2011, 28(5): 41 (in Chinese)

10 Gao Fan, Wang Xinying, Wang Lei *et al*. *Special Casting & Nonferrous Alloys*[J], 2011, 31(7): 608 (in Chinese)

11 Luo Wenzhong, Zhao Xiaohua, Liu Peng *et al*. *Rare Metal Materials and Engineering*[J], 2020, 49(3): 927 (in Chinese)

12 Li Pengfei, Li Jinshan, Sun Chang *et al*. *Iron Steel Vanadium Titanium*[J], 2013, 34(2): 24 (in Chinese)

13 Zhao Xiaohua, Li Jinshan, Yang Zhijun *et al*. *Special Casting & Nonferrous Alloys*[J], 2010, 30(11): 1001 (in Chinese)

14 Zhang Yingjuan, Kou Hongchao, Li Pengfei *et al*. *Special Casting & Nonferrous Alloys*[J], 2012, 32(5): 418

15 Fan Kai, Wu Lincai, Li Junjie *et al*. *Rare Metal Materials and Engineering*[J], 2016, 45(9): 2282 (in Chinese)

16 Kondrashov E N, Musatov M I, Maksimov A Y *et al*. *Journal of Engineering Thermophysics*[J], 2007, 16(1): 19

17 Boivineau M, Cagran C, Doytier D *et al*. *International Journal of Thermophysics*[J], 2006, 27(2): 507


# 钛合金TC4真空自耗熔炼工艺参数对宏观偏析影响


靖振权[1]，孙彦辉[1]，刘　睿[1]，陈　炼[2]，耿乃涛[3]，郑友平[3]，彭　力[3]，王　莹[3]

(1. 北京科技大学 钢铁共性技术协同创新中心，北京 100083)

(2. 攀钢集团攀枝花钢铁研究院有限公司，四川 攀枝花 617000)

(3. 成都先进金属材料产业技术研究院股份有限公司，四川 成都 610300)



**摘　要：**采用Fluent软件模拟了钛合金TC4真空自耗熔炼过程中温度场、流场和溶质场相互作用，研究了与铸锭直接相关的3个工艺参数（熔速、铸锭上表面温度和冷却强度）对铸锭宏观偏析的影响规律。结果表明：不同熔炼条件下，在铸锭1000 mm高度处的铁元素径向偏析均呈钟形分布，即铸锭芯部为正偏析，表面区域为负偏析，且负偏析程度均大于正偏析。熔炼速度对铸锭温度场和宏观偏析的影响最为明显：当熔炼速度由0.15 mm/s增加到0.18 mm/s时，铸锭达到稳定熔炼阶段时的高度由1200 mm增加到1600 mm，熔池深度由494 mm增加到738 mm。当距铸锭中心距离小于130 mm时，偏析随熔炼速度增加而减小，在熔炼速度为0.15 mm/s时达到最大值，为3.36%；当距铸锭中心距离大于295 mm时，偏析随熔炼速度增大而增大，在熔炼速度为0.21 mm/s时达到最大值6.23%。铸锭上表面温度和冷却强度对宏观偏析和熔池深度的影响不明显。通过正交分析得到3个主要工艺参数对宏观偏析影响程度为：熔炼速度＞冷却强度＞铸锭上表面温度，并得到最优工艺参数为熔炼速度0.15 mm/s、铸锭上表面温度2179 K、冷却强度500（底部）/1000（侧面）$W\cdot m^{-2}\cdot K^{-1}$。



**关键词：**钛合金；真空自耗熔炼；数值模拟；宏观偏析



作者简介：靖振权，男，1985年生，博士，北京科技大学钢铁共性技术协同创新中心，北京 100083，E-mail：jingzhenquan@126.com